Monthly Notices
of the
ROYAL ASTRONOMICAL SOCIETY

Mon. Not. R. Astron. Soc. **401,** 418–432 (2010) doi:10.1111/j.1365-2966.2009.15659.x

CoRoT photometry and high-resolution spectroscopy of the interacting eclipsing binary AU Monocerotis⋆

M. Desmet,[1]† Y. Frémat,[2] F. Baudin,[3] P. Harmanec,[4] P. Lampens,[2] E. Janot Pacheco,[5] M. Briquet,[1] P. Degroote,[1] C. Neiner,[6] P. Mathias,[7] E. Poretti,[8] M. Rainer,[8] K. Uytterhoeven,[8,9] P. J. Amado,[10] J.-C. Valtier,[7] A. Prša,[11,12] C. Maceroni[13] and C. Aerts[1,14]

[1]*Instituut voor Sterrenkunde, K.U.Leuven, Celestijnenlaan 200 D, B-3001 Leuven, Belgium*
[2]*Royal Observatory of Belgium, 3 Avenue circulaire, B-1180 Brussels, Belgium*
[3]*Institut d'Astrophysique Spatiale, CNRS/Université Paris XI UMR 8617, 91405 Orsay, France*
[4]*Astronomical Institute of the Charles University, Faculty of Mathematics and Physics, V Holešovičkách 2, CZ-180 00 Praha 8, Czech Republic*
[5]*Universidade de São Paulo, Instituto de Astronomia, Geofísica e Ciências Atmosféricas - IAG, Departamento de Astronomia, Rua do Matão, 1226 – 05508-900 São Paulo, Brazil*
[6]*Observatoire de Paris – Section de Meudon, Place Jules Janssen 5, 92195 Meudon cedex, France*
[7]*UNS, CNRS, OCA, Campus Valrose, UMR 6525 H. Fizeau, F-06108 Nice Cedex 2, France*
[8]*INAF – Osservatorio Astronomico di Brera, via Bianchi 46, 23807 Merate (LC), Italy*
[9]*Laboratoire AIM, CEA/DSM-CNRS-Université Paris Diderot; CEA, IRFU, SAp, Centre de Saclay, F-91191 Gif-sur-Yvette, France*
[10]*Instituto de Astrofísica de Andalucía (CSIC), Granada, Spain*
[11]*Villanova University, Dept. Astron. Astrophys., 800 E Lancaster Ave, Villanova, PA 19085, USA*
[12]*University of Ljubljana, Department of Physics, Jadranska 19, SI-1000 Ljubljana, Slovenia*
[13]*Osservatorio Astronomico di Roma, via Frascati 33, I-00040 Monteporzio (RM), Italy*
[14]*Department of Astrophysics, IMAPP, Radboud University Nijmegen, PO Box 9010, 6500 GL Nijmegen, the Netherlands*

Accepted 2009 September 2. Received 2009 September 2; in original form 2009 May 6

ABSTRACT

Analyses of very accurate CoRoT space photometry, past Johnson *V* photoelectric photometry and high-resolution echelle spectra led to the determination of improved and consistent fundamental stellar properties of both components of AU Monocerotis. We derived new, accurate ephemerides for both the orbital motion (with a period of $11\overset{\mathrm{d}}{.}113$) and the long-term, overall brightness variation (with a period of $416\overset{\mathrm{d}}{.}9$) of this strongly interacting Be + G semi-detached binary. It is shown that this long-term variation must be due to attenuation of the total light by some variable circumbinary material. We derived the binary mass ratio $M_{\mathrm{G}}/M_{\mathrm{B}} = 0.17 \pm 0.03$ based on the assumption that the G-type secondary fills its Roche lobe and rotates synchronously. Using this value of the mass ratio as well as the radial velocities of the G-star, we obtained a consistent light curve model and improved estimates of the stellar masses, radii, luminosities and effective temperatures. We demonstrate that the observed lines of the B-type primary may not be of photospheric origin. We also discover rapid and periodic light changes visible in the high-quality residual CoRoT light curves. AU Mon is put into perspective by a comparison with known binaries exhibiting long-term cyclic light changes.

Key words: accretion, accretion discs – binaries: general – binaries: eclipsing – stars: emission-line, Be – stars: individual: AU Mon.

⋆Based on photometry collected by the CoRoT space mission as well as spectroscopy obtained with the FEROS spectrograph attached to the 2.2-m telescope at European Southern Observatory (ESO), La Silla, Chile, under the ESO Large Programme LP178.D-0361, and with the SOPHIE spectrograph of the Observatoire de Haute-Provence (France). The CoRoT space mission was developed and is operated by the French space agency CNES, with the participation of ESA's RSSD and Science Programmes, Austria, Belgium, Brazil, Germany and Spain. Based on observations collected at the Centro Astronómico Hispano Alemán (CAHA) at Calar Alto, operated jointly by the Max-Planck-Institut für Astronomie and the Instituto de Astrofísica de Andalucía (CSIC).

†E-mail: maarten.desmet@ster.kuleuven.be

1 INTRODUCTION

AU Monocerotis (AU Mon) was selected as one of the few known binary targets in the asteroseismology field of the French-European CoRoT space mission (Convection, Rotation and Planetary Transits; Fridlund et al. 2006, see 'the CoRoT book') during the Initial Run (IRa01). We present here a detailed study of AU Mon based on a long, uninterrupted series of high-precision CoRoT photometry obtained in 2008 as well as on high-dispersion echelle spectra secured at three ground-based observatories in 2007.

AU Mon (HD 50846, HIP 33237) is an interacting, eclipsing and double-lined spectroscopic binary consisting of a Be star and an evolved late-type giant star which in all probability fills its Roche lobe and loses matter towards the Be star. To avoid confusion, we will hereafter denote the mass-gaining and the mass-losing components of AU Mon as the B- and G-stars, respectively (we will indeed demonstrate that the cool component is a G-type star rather than an F-type star which was its classification based on photographic spectra.). The orbit is circular and the orbital period is $11\overset{\mathrm{d}}{.}113\,02$ (see O − C diagrams[1] of Kreiner 2004). AU Mon is a rare Algol-type system member of the W Serpentis subclass, phenomenologically defined by Plavec & Koch (1978) and Plavec, Popper & Ulrich (1980). These binaries are sometimes also called 'massive or hot Algols'. According to current knowledge, they are characterized by a semidetached configuration and several distinct components of circumstellar matter: a 'cloud' of very hot plasma manifesting itself by emission lines in far-ultraviolet (far-UV) spectra and probably located outside the orbital plane, a disc, possibly optically thick, which mimics a false photosphere with a lower $T_{\rm eff}$ than the central star, a gas stream between both components and a 'hot-line region' arising from the interaction of the gas stream and the disc/cloud complex (Bisikalo & Matsuda 2007). We mention only some published studies of W Ser binaries, relevant to our present work. Elias (1990) studied centimetre observations of six different W Ser binaries and found very strong evidence for circumstellar matter around these systems. The same was claimed for SX Cas (Andersen, Pavlovski & Piirola 1989) and RX Cas (Andersen et al. 1989) on the basis of photometry and spectroscopy. A system which is similar to AU Mon is W Cru, consisting of a B-star and a G-supergiant. Pavlovski, Burki & Mimica (2006) found this object to have a very extended accretion disc with a clumpy rim, and suggested that the clumpiness may account for the light curve distortions and asymmetries as well as for secular changes.

2 PREVIOUS KNOWLEDGE ABOUT AU MON

2.1 Light changes, orbital period and ephemeris

The eclipsing nature of AU Mon was discovered by Hoffmeister (1931). The first ephemeris was published by Florja (1937). Lause (1938) derived a slightly longer value of the period. Lorenzi (1977) observed it and concluded that its light curve was undergoing rapid cyclic changes. He suggested that this could be due to a fast apsidal motion with a period of $243\overset{\mathrm{d}}{.}2$ but also pointed out problems with such an interpretation. Shortly thereafter, Cerruti-Sola & Lorenzi (1977) came up with the correct explanation: the brightness of the whole system varied secularly. To understand the phenomenon, Lorenzi (1980b) secured 2616 *V* differential observations between 1976 and 1979 at two observatories. From a detailed analysis of these data, Lorenzi (1980a) determined that the brightness of AU Mon varied cyclically with a period of 411 days and a peak-to-peak amplitude of about $0\overset{\mathrm{m}}{.}2$. Taking this variation into account, he derived an improved ephemeris for the binary system:

$$T_{\rm Min\,I} = \mathrm{JD}\,244\,2801.3752(51) + 11\overset{\mathrm{d}}{.}113\,0371(68) \times E, \qquad (1)$$

which has since been used by various other investigators. Lorenzi (1985) analysed new observations from 1983 and 1984 and confirmed the periodic character of the brightness variations of AU Mon. A regularly updated ephemeris, based on all compiled times of minima, can be found in the data base of the O − C diagrams (Kreiner 2004).[1]

2.2 Spectroscopic investigations

The first spectroscopic study aimed at the determination of the orbital elements was carried out by Sahade & Cesco (1945). Helped in the spectral classification by Dr. Morgan, they concluded from the spectra, at maximum light and during the eclipse, that the primary is a B5 main-sequence star and the secondary has a spectral class near F0. In a later study, Sahade & Ferrer (1982) investigated not only ground-based but also the far-UV spectra of the binary obtained with the *International Ultraviolet Explorer* (*IUE*). Faint lines of the secondary were detected in the Na I 5889 and 5895 Å doublet (Popper 1962) and later on measured quantitatively (Popper 1989). Popper (1962) also noted the presence of a double Hα emission. The first study, partly based on electronic spectra, was published by Sahade et al. (1997). A previous determinations of the orbital elements of AU Mon is listed in Table 1.

The far-UV spectra of AU Mon were obtained by *IUE* and studied by Polidan & Peters (1982), Peters & Polidan (1982), Peters (1988), Egikyan (1989), Peters (1991, 1994a,b, 1996) and Peters & Polidan (1998). Peters & Polidan (1982) confirmed that the gas stream between the components is seen in the UV resonance lines of N V and C IV in the orbital phase range 0.85–0.93, where phase zero corresponds to the time of primary eclipse. Egikyan (1989) found the electron density of the gas in the envelope to be $n_{\rm e} \sim 2 \cdot 10^{11}\,\mathrm{cm}^{-3}$, and the electron temperature to be $T_{\rm e} \sim 20\,000$ K. Peters (1988) found a correlation between the instantaneous mass transfer rate and the line and continuum spectrum along the 411-d cycle. At the maximum of the mass transfer rate, the object was fainter and the accretion disc denser while, at the brightness maximum, the high-temperature plasma was more prominent in the UV spectral lines. Analysing the spectral energy distribution (SED) from the low-dispersion *IUE* spectra, Peters (1991) concluded that the optical brightness variations of the system are due to a 1200 K variation in the photospheric effective temperature of the Be

Table 1. Spectroscopic orbital elements for AU Mon derived by Sahade et al. (1997) in a spectroscopic analysis.

Element	Value
$a_{\rm B} \sin i$ (10^6 km)	6.6 ± 0.39
$a_{\rm G} \sin i$ (10^6 km)	2.2 ± 0.41
$K_{\rm B}$ (km s^{-1})	43 ± 2.5
$K_{\rm G}$ (km s^{-1})	147 ± 3.0
e	0.06 ± 0.02
ω (°)	204 ± 22
γ (km s^{-1})	2.1 ± 1.5
$M_{\rm B}$ ($M_\odot$)	6.1 ± 0.61
$M_{\rm G}$ ($M_\odot$)	1.8 ± 0.53

[1] http://www.as.wsp.krakow.pl/o-c/index.php3

primary. She also suggested the presence of a 10 000 K continuum source from an optically thick accretion disc around the primary to model the SED. Peters (1994a,b) increased the estimate of the temperature of that source to 12 000 K and suggested that the cyclic variations in the mass transfer rate could be due to pulsation of the mass-losing secondary. Peters & Polidan (1998) obtained a single high-dispersion ORFEUS–SPAS II far-UV spectrum (920–1210 Å) and concluded that it is typical of a B3 V star [the SED including the *IUE* data can well be fitted with $T_{\rm eff} = 17\,000$ K and $\log g = 4.0$ (cgs)] with $v \sin i = 120$ km s^{-1}.

Richards & Albright (1999) made an in-depth study of the types of accretion structures found in Algol systems. AU Mon was part of their Hα spectroscopic study. They have put AU Mon in the group with a widely separated double-peaked disc-like structure. They have permanent, but variable, accretion discs similar to those found in cataclysmic variables. Miller, Budaj & Richards (2005) studied the properties of the accretion structures in AU Mon through a multiwavelength spectral study. Double-peaked emission was detected in the observed Hα line confirming the presence of an enduring accretion disc. The strength of the emission varies with epoch.

In a careful study, Glazunova et al. (2008) derived new rotational velocities for the components of 23 close detached and semidetached binaries. For AU Mon, they showed how the presence of circumstellar matter can falsify the determination of the projected rotational velocities. They attempted to avoid the problem and obtained $v_{\rm B} \sin i = 124 \pm 4$ km s^{-1} and $v_{\rm G} \sin i = 42.1 \pm 2.1$ km s^{-1}. They also derived the asynchronicity parameter of the B-star, $F_{\rm B} = 5.2$.

2.3 Published light curve solutions

To date, a few detailed photometric studies of AU Mon have been published. Several attempts, all of which are based on Lorenzi's observations pre-whitened for the 411-day variation, were made to derive light curve solutions, Lorenzi (1982) himself made the first attempt, creating symmetric normal points from his light curve and using the Russell–Merrill method. Independently, and a few months before him, Giuricin, Mardirossian & Mezzetti (1982) solved the light curve using Wood's model. Finally, another solution, this time based on the Wilson–Devinney (WD) method (Wilson & Devinney 1971; Wilson 1994), was published by Vivekananda Rao & Sarma (1998). These authors concluded that no third light is present in the system. The main results of these studies are summarized in Table 2. We note a good agreement between the first and the third solution, which are based on two independent computer programs.

Table 2. Published light curve solutions based on Lorenzi's (1980b) observations.

Element	GGM82	L82	VRS98
i (°)	78.4 ± 0.5	80 assumed	78.74 ± 0.06
$r_{\rm B}$	0.115 ± 0.013	0.18	0.131 ± 0.001
$r_{\rm F}$	–	0.18	–
$a_{\rm F}$	0.267 ± 0.056	–	0.2741 ± 0.0034
$b_{\rm F}$	0.242 ± 0.038	–	0.2417 ± 0.003
$c_{\rm F}$	0.232 ± 0.031	–	0.2324 ± 0.0031
$T_{\rm eff}$ (B eq.) (K)	15 000 assumed	15 500 assumed	$14\,500 \pm 1000$
$T_{\rm eff}$ (B pole) (K)	15 010	–	–
$T_{\rm eff}$ (F eq.) (K)	$6\,600 \pm 150$	5300	6000 ± 40
$T_{\rm eff}$ (F pole) (K)	16 860	–	–
q	0.2	–	0.1985
$L_{\rm B}$	0.645	0.93	0.6590 ± 0.0051
$L_{\rm F}$	0.355	0.07	0.3410

Note. The symbol $q = M_{\rm F}/M_{\rm B}$ stands for the mass ratio while the symbols a, b and c denote the relative dimensions of the triaxial ellipsoids, and the back, side and pole radii for the WD model. The following codes are used to identify the authors: GMM82 – Giuricin et al. (1982); L82 – Lorenzi (1982); VRS98 – Vivekananda Rao & Sarma (1998).

Table 3. The 6 new times of minima for AU Mon derived from the CoRoT data. The O − C values were calculated with our new ephemeris (2) for AU Mon.

Time (BJD 245 4000)	O − C
136.670 03(1)	−0.003
147.776 25(1)	−0.010
158.895 21(1)	−0.004
170.008 28(2)	−0.004
181.126 61(1)	0.001
192.237 62(2)	−0.001

3 THE NEW PHOTOMETRIC DATA AND THEIR ANALYSIS

The new photometric data set consists of a continuous series of 139 704 individual CoRoT photometric observations spanning an interval of 56 days, i.e. five orbital periods.[2] The spectral domain of CoRoT enfolds the range from 370 to 950 nm, the average time sampling was 32 s and roughly 10 per cent of the data points were deleted because they were extreme outliers. An estimate of the noise level of the light curve, computed as the average of the periodogram between 80 and 120 d^{-1} is 60 μmag. In addition to the CoRoT data, we critically compiled and homogenized all published photoelectric observations with known dates of observations as well as all available times of minima known to us and derived six new times of primary minima from the CoRoT light curve. Table 3 lists the six new CoRoT minima. The published visual, photographic, photoelectric and CCD times of minima, reproduced in Table A1, were obtained from the General Search Gateway of the Variable-Star Section of the Czech Astronomical Society[3] where also references to original observers can be found.

3.1 Time-series analysis and new ephemeris

Fig. 1 shows the complete set of CoRoT observations versus HJD. We converted CoRoT fluxes (F) to magnitudes (m) using $m = -2.5 \log F + C_0$, with C_0 a calibration constant. We derived C_0 through a comparison between CoRoT magnitudes and visual magnitudes from literature for all constant stars in the CoRoT field of AU Mon. This gives a value of $C_0 = 23.16 \pm 0.05$ mag.

First, we verified that Lorenzi's ephemeris (1) can reconcile both the compiled published photometry and the CoRoT data. Consequently, we used his ephemeris for the initial analyses. In the final modelling of photometry and radial velocities (RVs) with the PHOEBE program, described in Section 5, we derived the following improved

[2] The CoRoT data of AU Mon are public and can be accessed at http://idoc-corot.ias.u-psud.fr/.

[3] http://var.astro.cz/gsg

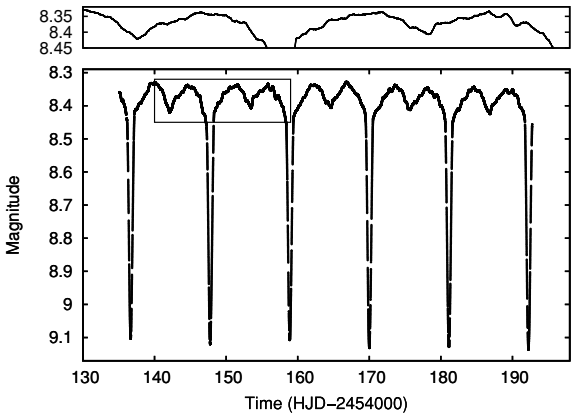

Figure 1. The complete CoRoT light curve of AU Mon. The upper panel shows an enlarged segment of the curve with very clear rapid non-orbital variations. The noise on the data is smaller than the symbol.

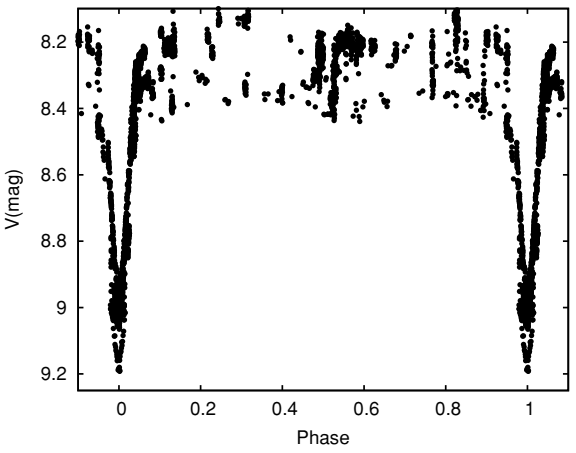

Figure 2. Original V-band light curve phased against the period of 11.113 0374 days.

orbital ephemeris

$$T_{\min \mathrm{I}} = \mathrm{HJD}\,245\,4136.6734(2) + 11\overset{\mathrm{d}}{.}113\,0374(1) \times E. \quad (2)$$

We collected all the available photoelectric observations of AU Mon and put them on to a comparable photometric system. The journal of all observations is shown in Table 4, the data itself can be found in Table B1. We converted the *uvby* data to Johnson *UBV* using the transformation derived by Harmanec & Božić (2001). The *Hipparcos* data were transformed to the V magnitude of the Johnson system using the transformation formula derived by Harmanec (1998). Fig. 2 shows the phased V light curve based on all the published observations we could collect from the literature, including the 2698 observations provided by Lorenzi (1980b, 1985). We can observe a systematic shift between two extreme states of the maximum light (at the levels of 8.2 and 8.4 mag, respectively) as well as of the primary minima (at the levels of 9.0 and 9.2, respectively). This effect is clearly due to the long-term periodicity reported by Lorenzi (1980a, 1985).

Subsequently, using subsets of V data sorted into narrow orbital-phase bins, as well as all the V data outside of the phase of primary minimum, we carried out a period search using the phase dispersion minimization (PDM) (Stellingwerf 1978) and the CLEAN (Roberts, Lehar & Dreher 1987) methods. Both algorithms yielded the same value of $P_{\mathrm{long}} = 417 \pm 8$ d. Fig. 3 shows the V magnitude outside minima plotted versus phase of the 417-day period. Our linear ephemeris for the total brightness of the system reads as follows:

$$T_{\mathrm{max\ tot\ brightness}} = \mathrm{HJD}\,244\,3105.1(\pm 1.4) + 416\overset{\mathrm{d}}{.}9(\pm 8\overset{\mathrm{d}}{.}7) \times E. \quad (3)$$

This also means that the CoRoT light curve was collected at a phase of total light minimum (in the phase range from 0.46 to 0.59).

The V-band light curves were inspected at the phases of light minima and maxima. The two curves are only shifted for about $0\overset{\mathrm{m}}{.}2$ with respect to each other (see Fig. 2) but have *the same shape and amplitude*, as already concluded by Cerruti-Sola & Lorenzi (1977). This was confirmed by tentative light curve solutions for both curves, which led to the same values of stellar radii and orbital inclination. This result does not support the idea promoted by Peters (1991) that the observed changes could be related to apparent changes in the T_{eff} and radius of the B-star's false photosphere. If the 417-day variation were caused by some variable third light then the eclipses should become shallower at the 417-day light maxima. Similarly, a precession of the orbit would lead to a changing orbital inclination. Since none of all these effects is present, we conclude that the long-term variation must be caused by a periodic attenuation of the total light of the binary by some variable circumbinary matter. The reason why we do not see emission lines coming from this circumbinary envelope might be that the envelope is cool and dusty. Probably, this huge envelope will also have a small rotational

Table 4. Journal of available photometry of AU Mon with known times of observations.

Station	Time interval (HJD 240 0000)	No. of observation	Passbands	HD of comparison /check star	Source
1	42790.3–42879.3	278	V	50109/50346	Lorenzi (1980b)
2	43023.6–43843.4	2143	V	50109/50346	Lorenzi (1980b)
3	43877.7–43880.9	195	V	50109/50346	Lorenzi (1980b)
4	44284.4–44287.4	13	$B-V$	All-sky	Kilkenny et al. (1985)
4	44288.3–44289.4	2	UBV	All-sky	Kilkenny et al. (1985)
4	44677.3–44678.3	2	UBV	All-sky	Kilkenny et al. (1985)
5	45254.9–45322.8	14	*uvby*	50747/50820	Manfroid et al. (1991)
2	45343.4–45790.4	82	V	50109/50346	Lorenzi (1985)
6	47987.4–49056.1	81	H_{p}	All-sky	Perryman & ESA (1997)
7	54136.0–54192.8	139 704	COR	All-sky	This paper, Corot

Individual observing stations and photometers distinguished by the running numbers in column *'Station'*:
1 – Torino Observatory 1.04-m reflector, EMI 9502 tube; 2 – Torino Observatory 0.60-m reflector, EMI 6256S tube; 3 – Cerro Tololo 0.40-m reflector, EMI 6256 tube; 4 – South African Astronomical Observatory 1.0- and 0.5-m telescopes, EMI 6256 and 9659 tubes; 5 – ESO La Silla telescope; 6 – *Hipparcos* satellite; 7 – Corot satellite.

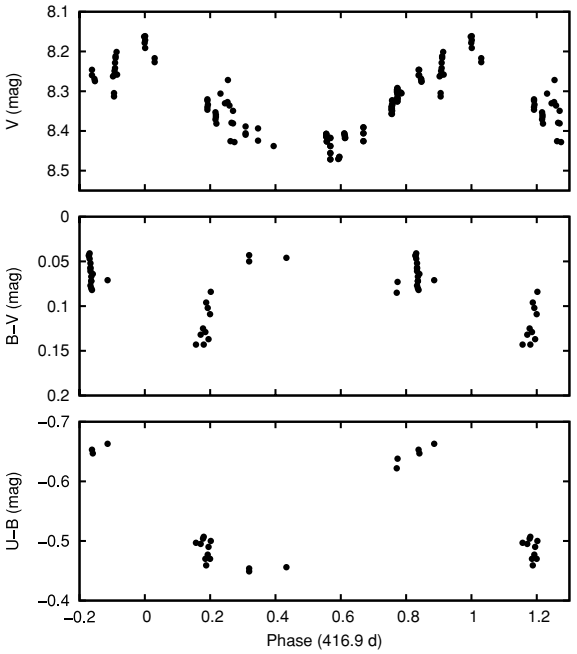

Figure 3. The V magnitude of AU Mon outside minima plotted versus phase of the 417-day period (top panel). The $B - V$ and $U - B$ colour changes along the 417-day cycle of AU Mon are shown in the middle and bottom panel (see Section 8 for details).

speed. Thus, its emission will be blended with the stronger emission from the circumstellar matter.

4 SPECTROSCOPIC ANALYSIS AND RADIAL VELOCITIES

4.1 Initial analysis of the spectra

New high-dispersion spectroscopic observations were obtained simultaneously with the CoRoT data over three consecutive orbital periods of AU Mon. They were carried out in the framework of the CoRoT ground-based follow-up programme (Uytterhoeven et al. 2008). The data we used here consist of 16 Fiber-fed Extended Range Optical Spectrograph (FEROS) echelle spectra ($R \sim 48\,000$; Kaufer et al. 1997, 1999) from the 2.2-m ESO/MPI telescope at La Silla, Chile, 11 well-exposed echelle spectra secured with the Spectrograph for Observation of Astroseismologic Phenomenon and Extrasolar Planets (SOPHIE) ($R \sim 70\,000$; Perruchot et al. 2008) attached to the 1.93-m telescope of the Haute Provence Observatory and four spectra taken with the Fibre Optics Cassegrain Echelle Spectrograph (FOCES; $R \sim 65\,000$; Pfeiffer et al. 1998) at Calar Alto Astronomical Observatory. The journal of observations, together with adopted RVs, is given in Table 5.

All data were subjected to the normal reduction process, which consists of debiasing, background subtraction, flat-fielding and wavelength calibration. All the reduced spectra were subsequently shifted to the heliocentric frame. Continuum rectification and cosmic-spike removal were carried out manually using the SPEFO program (Horn et al. 1996; Škoda 1996), written by the late Dr. Jiří Horn and until recently being developed by Mr. J. Krpata.[4]

To have some guidance before application of more sophisticated methods, we first derived the RVs via classical measurements. Using the program SPEFO, we carefully rectified all red parts of the spectra (between 5500 and 6700 Å) and cleaned them from cosmics and flaws. The RVs of both components were then measured comparing the direct and flipped line profiles. For the G-star, we measured Ca I 6102.723 Å, Fe I 6141.730 Å and Fe I 6400.000 Å which are all well-defined, unblended and relatively strong spectral lines. The rms errors of the mean RV of these three lines ranged from 1 to 4 km s^{-1}. The corresponding orbital RV curve is shown by black circles in Fig. 4. The only strong and unblended line which seems to be related to the B-star in the studied red wavelength range is He I 5875.732 Å (open circles in Fig. 4). For the Hα line (red dots in Fig. 4), the setting was made on the steep wings of the double emission and the measurements were carried out only when a reliable setting was possible.

The RV curve of the G-star is well defined and appears sinusoidal. To check on the presence of a possible small eccentricity, we first derived trial solutions for an elliptical orbit using the programs SPEL (unpublished, written by the late Dr. Jíří Horn) and FOTEL (Hadrava 1990, 2004a). We obtained $e = 0.045 \pm 0.006$, $\omega = 93\overset{\circ}{.}5 \pm 7\overset{\circ}{.}2$ and $K_{\rm G} = 156.71 \pm 0.92$ km s^{-1}, and the test suggested by Lucy & Sweeney (1971) indicated that the eccentricity is significant. However, we do believe that the orbit *is circular* and the eccentricity *is spurious*, caused by a small difference between the photocentre of the Roche lobe filling star and its centre of gravity and/or by the Rossiter–McLaughlin (RM) effect (as detailed in Section 6). It was pointed out by Harmanec (2001, 2003) that any disturbance of the sinusoidal shape of the RV curve which is symmetric with respect to the systemic velocity *must lead to a formally eccentric orbit* with a longitude of periastron of either 90° or 270°. This is exactly what we found. Note also that for these orientations of the binary orbit, the photometric minima are separated for exactly one half of the orbital period so that even very accurate photometry cannot provide an additional test.

Using FOTEL (Hadrava 1990, 2004a), we therefore derived a trial circular orbit solution for the G-star, which is compared to formal solutions for the RVs of the Hα emission wings and He I 5876 Å absorption in Table 6. The epoch of the primary minimum derived from the G-star RVs agrees with that of (photometric) ephemeris (2). In contrast to this, the RV curve of the He I 5876 Å absorption and Hα emission are mutually similar but shifted in phase with respect to the clean antiphase orbital motion of the G-component. Popper (1989) also suggested such behaviour. All this is the situation reminiscent of another W Ser star with a similar orbital period of $12\overset{\rm d}{.}9$, namely β Lyr, where such a behaviour is due to the fact that the absorption and emission lines originate in bipolar jets emanating from the region of interaction of the gas streams (Harmanec et al. 1996). This may imply that we do not see really photospheric lines of the hot mass-gaining star of AU Mon.

4.2 Mass ratio and secondary mass

To cope with the above problem, we attempted to obtain some estimate of the mass ratio independent of the B-star's RV curve. Since the contact components of semidetached binaries usually rotate synchronously with their revolution (see e.g. Harmanec 1988), we made this assumption also for AU Mon and used the procedure devised by Andersen et al. (1989) as detailed in the appendix of Harmanec (1990) to obtain an independent estimate of the mass ratio (q), component masses and the radius ($R_{\rm G}$) of the Roche lobe filling secondary. Its principle lies in the fact that the relative dimensions of the Roche lobe depend solely on the binary mass ratio q while the absolute radius of the spin–orbit synchronized secondary

[4] Mr. J. Krpata passed away on 2006 February 6.

Table 5. RVs measured from the FEROS (FE), SOPHIE (SO) and FOCES (FO) data.

HJD 245 4000	S/N	RV_B (km s^{-1})	RV_G (km s^{-1})	$RV_{He\,I}$ (km s^{-1})	RV_G (km s^{-1})	$RV_{H\alpha}$ (km s^{-1})	I.
76.6493	95	23.3 ± 4.2	−76.74± 3.60	41.4	−76.3	13.0	FO
76.6697	112	26.6 ± 3.1	−80.23 ± 4.06	42.7	−78.7	16.0	FO
78.6665	86	49.8 ± 4.4	−129.55 ± 3.15	78.2	−121.2	33.1	FO
78.6902	86	59.5 ± 6.2	−128.60 ± 2.84	91.3	−127.0	43.8	FO
103.7806	117	−6.553 ± 6.939	55.94 ± 1.73	26.9	56.4	−2.7	FE
104.6490	105	−2.108 ± 10.153	121.79 ± 1.04	0.6	124.8	14.2	FE
104.8285	98	−7.657 ± 8.524	132.61 ± 1.36	14.0	137.3	11.2	FE
105.6557	107	−14.990 ± 9.559	168.19 ± 3.30	−7.5	175.2	1.7	FE
105.8796	118	−15.247 ± 8.629	172.65 ± 2.37	−20.1	174.6	3.4	FE
106.6320	76	−14.334 ± 7.206	171.27 ± 1.57	1.9	173.4	6.1	FE
106.8208	103	−16.287 ± 6.911	164.85 ± 1.78	−17.3	168.3	9.1	FE
107.7008	124	−10.859 ± 4.584	125.02 ± 2.30	−10.3	126.1	−24.3	FE
108.7038	129	−2.453 ± 0.644	42.17 ± 4.11	2.0	44.6	1.2	FE
108.8141	101	3.384 ± 3.488	28.12 ± 3.99	3.0	30.2	−5.2	FE
108.8739	159	0.963 ± 2.589	18.01 ± 11.45	1.8	26.1	−6.7	FE
109.6744	93	16.264 ± 4.232	−57.97 ± 2.87	23.1	−55.0	15.1	FE
110.5600	125	36.924 ± 3.668	−111.92 ± 2.67	35.7	−105.7	27.2	FE
113.3762	72	26.498 ± 3.610	−65.29 ± 1.88	51.9	−59.4	74.2	SO
114.3554	38	19.044 ± 5.689	12.74 ± 1.48	90.7	15.2	61.4	SO
115.3513	41	−2.481 ± 4.473	94.00 ± 2.63	20.3	92.5	30.7	SO
118.3702	60	−13.448 ± 7.440	150.47 ± 2.79	−26.5	150.7	−2.8	SO
119.4596	53	−5.039 ± 5.894	79.44 ± 3.00	−13.3	90.6	−23.9	SO
121.3731	59	26.867 ± 7.542	−95.42 ± 3.96	18.2	−88.1	41.3	SO
125.7931	99	−37.327 ± 7.089	37.10 ± 2.34	7.2	41.0	31.6	FE
127.6520	103	−12.026 ± 9.820	161.75 ± 1.50	2.2	164.5	2.0	FE
128.3489	58	−9.204 ± 2.343	174.38 ± 1.69	7.5	177.8	–	SO
128.6499	115	−13.868 ± 7.290	174.36 ± 2.42	−2.2	177.3	−10.0	FE
129.3422	64	−13.363 ± 6.859	155.57 ± 2.06	−6.6	158.1	−16.8	SO
130.3320	62	−2.870 ± 7.891	98.79 ± 1.55	2.5	98.4	−28.0	SO
131.3412	69	8.946 ± 1.713	−9.75 ± 4.66	5.8	−2.3	0.2	SO
132.3469	57	27.212 ± 6.149	−87.30 ± 1.37	18.5	−85.9	19.4	SO

Note. The RVs of the G-star were derived via 1D cross-correlation of suitable parts of the red wavelength region while the B-star RVs were derived near 4000 Å using a 2D TODCOR-type cross-correlation. The last three RV columns are the measurements carried out in SPEFO – see the text for details. The last column denotes the instrument.

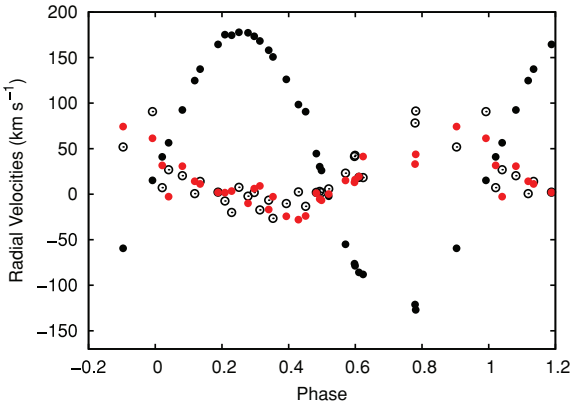

Figure 4. The RV curves of the late-type G-spectrum (black dots), B-spectrum (open circles) and the Hα emission wings (red dots) measured in SPEFO. One can see that the B-spectrum RV, based on the He I 5876 Å, and that of the Hα emission wings define similar RV curves which are both shifted in phase with respect to the expected RV curve of the G-component.

Table 6. Trial circular orbit solutions for the direct RV measurements in SPEFO (top). FOTEL circular orbit solutions for the RV measurements via cross-correlation of selected segments of the spectra as described in Section 4.4 and tabulated in Table 5 (bottom). The orbital period was kept fixed at $11^{\rm d}.113\,0374$. The epoch of the primary minimum is in HJD 245 4000, rms is the rms error of 1 observation.

Element	G-star mean RV	Hα emission wings	He I absorption
$T_{\rm min\,I}$	136.668 ± 0.018	137.94 ± 0.17	137.46 ± 0.13
K (km s^{-1})	157.64 ± 0.16	32.7 ± 1.7	38.6 ± 1.4
γ (km s^{-1})	22.3 ± 1.2	19.4 ± 2.4	23.3 ± 2.4
rms (km s^{-1})	6.19	12.4	12.0

Element	G-star mean RV	B-star mean RV
$T_{\rm min\,I}$	136.684 ± 0.016	136.972 ± 0.086
K (km s^{-1})	158.51 ± 0.14	30.41 ± 0.79
γ (km s^{-1})	18.8 ± 1.1	12.2 ± 1.1
rms (km s^{-1})	5.47	5.98

is uniquely given by its equatorial rotational velocity, inclination i of its rotational axis (assumed to be identical to the inclination of the orbit) and the rotational (=orbital) period. The binary separation is given by the third Kepler law so that there is only one mass ratio for which the secondary is just filling the corresponding Roche lobe. We assumed a circular orbit, $K_{\rm G} = 158 \pm 1$ km s^{-1} and a range of orbital inclinations from 77° to 83° (see Section 5). We took the uncertainties of the parameters $K_{\rm G}$, $v \sin i$ and $P_{\rm orb.}$ (used

Table 7. Basic properties of AU Mon estimated from spectroscopy (see the text for details).

	B-star	G-star
$T_{\rm eff}$	$15\,000 \pm 2000$ K	5750 ± 250 K
$\log g$	3.5 ± 0.3	–
M	$6.37^{+2.18}_{-1.12}$ M$_\odot$	$1.17^{+0.19}_{-0.19}$ M$_\odot$
R	$7.15^{+5.77}_{-2.92}$ R$_\odot$	$9.7^{+0.6}_{-0.6}$ R$_\odot$
$V_{\rm eq.}^{\rm synch.}$	32^{+26}_{-13} km s^{-1}	–
$v \sin i$	116 ± 2 km s^{-1}	43.8 ± 3.5 km s^{-1}
$q = M_{\rm G}/M_{\rm B}$	$0.17^{+0.03}_{-0.03}$	

Note. The values of $v \sin i$ were derived using the disentangled spectra (see Section 4.3), the semi-amplitude $K_{\rm G} = 157$–159 km s^{-1} was derived from our spectra and the orbital inclination was assumed to be in the range from 77° to 83° (see Section 5).

in the procedure) into account to provide the error estimates of the resulting values of q, $M_{\rm G}$ and $R_{\rm G}$. The results are listed in Table 7. The mass ratio of AU Mon equals $q = 0.17 \pm 0.03$. Our results agree with Vivekananda Rao & Sarma (1998, see Table 2). Sahade et al. (1997) found a mass ratio of $q = 0.29$ which is much larger compared to any other study. This is due to their usage of the value of $K_{\rm B}$, which is probably too optimistic. As Fig. 7 shows, their B-spectrum RVs, from phase 0.0 to 0.5, are much more negative than any other recorded RVs. Moreover, our separate circular orbit solutions for their B- and G-spectrum RVs give systemic velocities of 1.6 ± 2.1 and 5.4 ± 3.3 km s^{-1}, differing quite substantially from the systemic velocity found by us and in all other previous studies.

4.3 Spectra disentangling and spectral type classification

To separate the spectra of both binary components in an objective way, we used the disentangling procedure developed by Hadrava (1995, 1997, 2004b, see references therein – Release 2.12.04 of the KOREL program made available to YF). The disentangling was applied to different parts of the spectra. The orbital period was fixed at the value derived by Lorenzi (1980a, see ephemeris (1) of this paper) and a circular orbit was assumed.

Within the parameter range we investigated, the disentangled spectra were sufficiently stable to permit to derive the projected rotation velocity and the effective temperature of both stars. We therefore disentangled the 5500–5700, 6125–6275 and 4000–4200 Å wavelength intervals. Eleven isolated lines were selected in the secondary's spectrum and two in the primary spectrum, and we estimated the components' $v \sin i$ by measuring the position of the first zero of the line profiles Fourier transform (FT; Royer et al. 2002). The values we found are given in Table 7 and are in good agreement with those measured by Glazunova et al. (2008), who tried to avoid the effects linked to the presence of the companion and of the circumstellar matter. Though our result for the primary is somewhat smaller, the difference is not significant regarding the scatter and the small number of lines available in fast rotating early-type stars to carry out such kind of analysis. We then compared the component spectra to synthetic ones, computed for different effective temperatures by means of the ATLAS local thermodynamic equilibrium model atmospheres (Castelli, Gratton & Kurucz 1997; Castelli & Kurucz 2003) and the SYNSPEC (Hubeny & Lanz 1995) program. This comparison was done in the red wavelength ranges for the secondary, while we mainly focused on the bluest range for the primary. Since the studied spectral ranges do not show any strong $\log(g)$ dependence, the surface gravity of the secondary (expected to be evolved) was fixed to $\log g = 2.5$.

Furthermore, we assumed a microturbulence of 2 km s^{-1} and a solar chemical composition. Since we used the hydrogen and helium stark-broadened line profiles for the B-star, our conclusions are in this case not significantly affected by these assumptions. For the G-star, spectra for different iron content (i.e. within 0.2 dex of the solar abundance) and within 2 km s^{-1} of the adopted microturbulent velocity were computed and analysed. The differences between the models with different iron abundances were found to be smaller than those obtained by using different effective temperatures within the estimated error bar of 250 K. Usually, a change in microturbulence affects more significantly the spectrum. However, the weaker lines which are present in the different wavelength ranges we have analysed, and falling in the linear part of the curve of growth, are not affected by a change in microturbulence. These lines were also used to estimate the effective temperature of the G-star and a good agreement was found between synthetic and observed spectra.

In Fig. 5, one can see the comparison between the disentangled and synthetic spectra for a selected wavelength range for the two components. The luminosity ratios we estimated in different wavelength domains are plotted in Fig. 6, while the astrophysical parameters we obtained are listed in Table 7. As a byproduct of the disentangling procedure, we obtained the RVs for both components (see Fig. 7). For comparison matters, we further assumed a non-perturbed stellar evolution and a solar-like metallicity. To determine the mass, radius and equatorial rotation velocity at orbit synchronization of the B-star, we made use of the evolutionary tracks calculated by Schaller et al. (1992). We interpolated the mass and radius for the effective temperature and surface gravity of

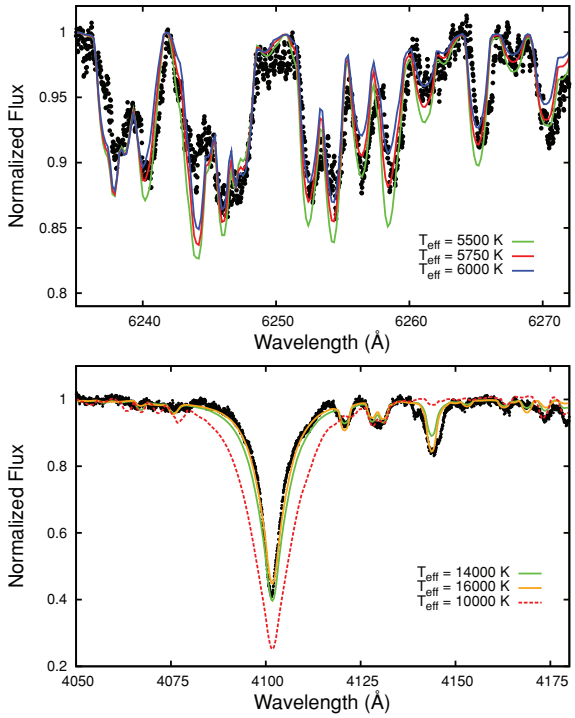

Figure 5. Comparison between synthetic spectra computed for different effective temperatures and the observed disentangled spectrum (black dots) of the cool G-component (upper panel) and the B-component (lower panel). The best-fitting temperatures for the G- and B-star are 5750 and 15 000 K, respectively. The absorption lines around 4070 Å are coming from an A0 spectrum (extended photosphere) and are best reproduced with a spectrum of 10 000 K.

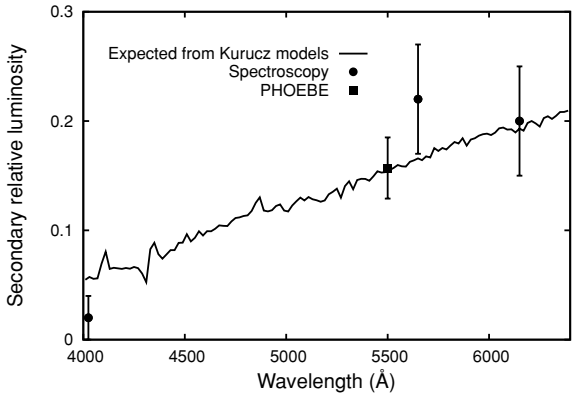

Figure 6. The expected wavelength dependence of the relative luminosity of the G-star to the total light of the system. We assumed effective temperatures of 15 000 and 5750 K for the B-primary and the G-secondary, respectively. The full line is based on Kurucz' models. The light contribution at 6150 Å was fixed at 0.2. The luminosity ratio was estimated from detailed comparisons of the observed and synthetic spectra at several distinct wavelength regions and these values are shown by black dots with errors. The black square with an error box represents the luminosity ratio in the *V* band based on the PHOEBE solution.

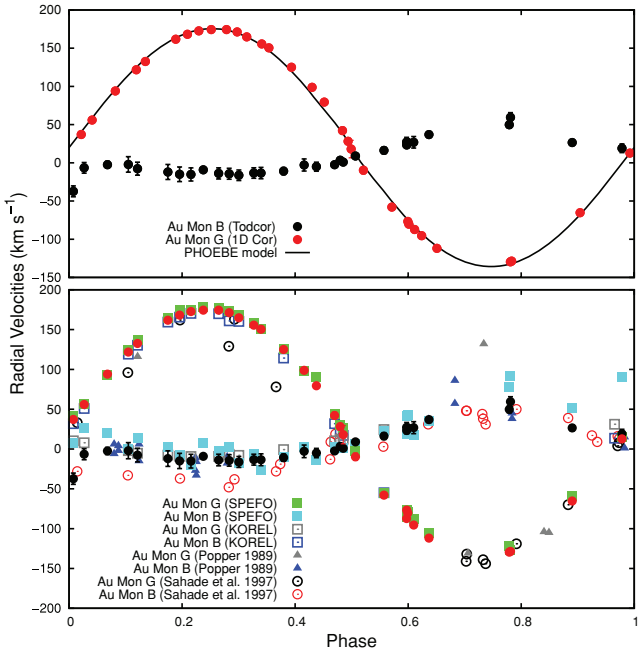

Figure 7. RVs obtained in this study by various methods (SPEFO, TODCOR, 1D CC, KOREL) compared to published values. The top panel shows our new and final RVs for sake of clarity and the bottom panel shows the comparison. The black line shows the final PHOEBE model for the G-star. The residuals for the G-star are pictured in Fig. 11.

the B-star throughout these evolutionary tracks. The results of this method can be seen in Table 7. The errors on M_B and R_B are unfortunately too large to determine the age of the star. Our result firmly establishes that the cooler star is a bright G-giant, and not an F-star as was tentatively classified in the past.

From the lower panel of Fig. 5, we see that the agreement between the best synthetic and observed spectra for the B-star is not perfect. The B-star spectrum is clearly affected by the circumstellar matter that acts like an extended photosphere and produces additional absorption lines generally found in A0 stars ($T_{\rm eff} \sim 10\,000$ K; spectral lines around 4075 Å are coming from the A0 star spectrum).

4.4 Determination of RVs from whole segments of spectra

Since the motion of the circumstellar matter seems to be phase locked with the orbital motion of the B-star, and the companion is a G-star with many weak but sharp spectral lines, the RV determination for the G-star is quite straightforward. To avoid systematic effects due to the presence of spectral lines belonging to the B-star, we concentrated on the 5500–5850 Å wavelength region and carried out *a 1D cross-correlation* of the observations with a synthetic spectrum computed for the stellar spectral classes derived in Section 4.3. (see David & Verschueren 1995, for the correlation maximum location). To estimate the accuracy of our measurements, the cross-correlation was performed separately on seven subparts of this spectral range, each subregion providing one set of RV measurements. In Table 5, we provide the mean RVs obtained from those seven regions and their rms errors.

Due to the orbiting circumstellar matter and the fewer lines present in the spectrum of early-type stars, the RVs of the B primary are much more difficult to measure. The systematic study of the whole available wavelength range shows a large scatter due to (1) the lack of spectral lines, (2) the presence of a *third spectrum* related to the matter orbiting the primary B-star (and showing lines generally formed in A0 stars) or/and (3) due to bipolar jets or disc/stream interactions (see Section 4). The best wavelength region candidate for the measurement of the primary's RVs is the one that encompassed the He I 4009 and 4026 Å lines where the effects of the (cooler) *third ('A0')* spectrum seem to be absent. Note that the G-star is more than 3 mag fainter at these wavelengths according to Fig. 6. Still, to reduce any systematic effect due to the faint G-star spectrum, we used a two-dimensional correlation (TODCOR)-like procedure (Zucker & Mazeh 1994) using templates that reflect the spectral types of the components (see Section 4.3). This operation was carried out several times using different templates for the primary, with the astrophysical parameters falling within 1σ of the estimated values in order to have an estimate of the accuracy of the procedure. The results are given in Table 5 and compared to other published measurements in Fig. 7.

We also derived FOTEL circular orbit solutions for these RVs. The results are shown in Table 6. One can see that the solution for the G-star agrees reasonably well with that based on the directly measured RVs (see Table 6). The solution for the B-star RVs again shows a phase shift with respect to the expected instant of the primary minimum and a significantly lower systemic velocity. The *K*-value for the B-star agrees within the errors with the *K*-value estimated from our principal analysis (see Table 6). Nevertheless, because of the phase and systematic velocity shift, we will not use the RV curve of the B-star in the determination of the binary physical properties.

5 MODELLING OF THE LIGHT AND RV DATA

In order to derive physical properties from the combined light and RV curves, we used the PHOEBE program, release 031dev (with phoebe-gui-cairo; Prša & Zwitter 2005) built on the 2003 WD method (Wilson & Devinney 1971; Wilson 1990), to perform the linearized least-squares analyses with the differential corrections approach. We assumed a semidetached system configuration (using Mode 5), and no third light or spots were included. *From previous considerations, we decided to rely only on the spectroscopic estimation of the mass ratio and the RVs of the G-star for this modelling.* We also fixed the effective temperature of the G-star at the value of

5750 K, since this value was reliably derived from the disentangled spectra (see Section 4.3).

The orbital period of $11\overset{\mathrm{d}}{.}113\,037$ was initially fixed. For the bolometric albedos, A_{B} and A_{G}, and the gravity darkening coefficient, G_{B}, we used their theoretical values corresponding to the type of atmosphere and to the spectral types of both stars (see e.g. Vučković et al. 2007). For the gravity darkening coefficient G_{G}, we had to adopt a value of 0.9, i.e. much higher than the theoretical value of 0.32, to obtain a satisfactory fit with the data. This value lies very close to the value expected for a radiative envelope. The limb darkening coefficients x and y of the B- and G-stars were taken from Castelli & Kurucz (2004) for the Johnson V curve while new limb-darkening coefficients specifically computed for the CoRoT passband, which are now implemented in PHOEBE (rel. 031dev), were used. The CoRoT limb-darkening coefficients were derived from a specific extension of the tables of van Hamme (1993) for the CoRoT transmission function (Fridlund et al. 2006), and computed by Van Hamme (private communication). The method is described in van Hamme (1993), it is a convolution of the outgoing intensities with the CoRoT transmission curve for different angles. The errors on x(CoR) and y(CoR) coming from this method are 0.001. The heliocentric Julian epoch of the primary minimum, HJD_0, the effective temperature of the B-star, $T_{\mathrm{eff.\,B}}$, the inclination, i, the dimensionless potential, Ω_{B}, the fractional luminosity of the B-star, L_{B}, the systematic velocity, γ, and the eccentricity, e, were all set as adjustable parameters. For the asynchronicity parameter, F_{B}, we used 4 ± 1 since the projected rotational velocity of the primary component appears to be approximately four times the estimated synchronous velocity (which amounts to $30 \pm 15\,\mathrm{km\,s^{-1}}$ if we adopt the B-star's radius from the solution presented below). We also checked whether leaving F_{B} as a free parameter improved our model. This was not the case.

For practical reasons mainly, we constructed 10 different subsets from the CoRoT light curve. Given that the CoRoT light curve of AU Mon was largely oversampled, we have split the continuous time series into 2×5 full orbital cycles selecting either even or odd data points in time, thus yielding 2×5 different CoRoT data subsets. In this way, no information was lost and we were able to obtain formal errors based on 10 independent subsets of the data. Thus, the 10 CoRoT data subsets, all the compiled V-magnitude photoelectric observations and the 1D cross-correlation RVs of the G-star from Table 5 were used in an iterative procedure to search for a consistent model. Of course, the CoRoT data are of much higher quality compared to the V-band light curve which is reflected in the scatter (uncertainties) on the data.

First, we simultaneously modelled each individual CoRoT data subset with the past V-band light curve. In this step, we used equal weights both for the CoRoT and the V-band data. This rapidly converged towards one possible light curve model obtained from averaging over the 10 found solutions. The mean parameters (computed with standard errors) were then adopted as the starting values for the next step in the modelling. Next, we simultaneously modelled each individual CoRoT data subset and the past V-band light curve together with the cross-correlation RVs of the G-star. The weights we assigned in this step to the photometry are now inversely proportional to the square of the rms errors for each data set. This means that the CoRoT data were given a much larger weight (0.98) than the V-band data (0.02) throughout these calculations. The reduced χ^2-values for each modelling approximated the value $\chi^2 = 1.4$ for the CoRoT subsets, and the fit for the V-band light curve had a value of $\chi^2 \approx 2.1$. Again, an improved light curve and RV model was obtained from averaging over the 10 found solutions.

Finally, we improved the orbital period and the epoch of primary minimum, HJD_0, of AU Mon using PHOEBE and our best-fitting model: we simultaneously fitted all the data with the orbital period and HJD_0 set as the only free parameters. This yielded a period of $11\overset{\mathrm{d}}{.}113\,0374(1)$, which is almost the same as the orbital period determined by Lorenzi (1980b) and which we adopted as a fixed parameter in our final modelling. The final value for HJD_0 is $\mathrm{HJD}_0 = 245\,4136.6734(2)$. We checked whether inclusion of third light in the modelling would improve our solution. This was not the case. We also verified that, when leaving the mass ratio q as a free parameter, its value was fully consistent with our spectroscopic estimate of q.

The mean parameters (with estimated uncertainties) and the resulting physical properties of both components are listed in Table 8. The true uncertainties will be larger because they depend on unknown systematic uncertainties and parameter dependencies which were not treated here. The observed V and CoRoT light curves and the synthetic model are shown in Fig. 8. There is a very good agreement between the CoRoT observations and the best-fitting model: the mean residual value in all the subsets is of the order of 0.02 mag (Fig. 9), though somewhat larger near the phase of primary minimum. We note, however, that the expected effective temperature for a normal main-sequence B-star with a mass of 7 solar masses would be higher than 15 000 K we obtained, in the order of 20 000–21 000 K. The radius of 5.6 solar radii also appears too large, even for the mass of 7 solar masses, it should be of the order of 4 solar radii. This may indicate that also from photometry one measures the outer radius of the optically thick pseudo-photosphere, rather than the true radius of the B-star. Seen roughly equator on, such a pseudo-photosphere would also have a lower effective temperature. Fig. 7 shows the PHOEBE model for the RVs of the G-star. Fig. 10 illustrates the configuration of the binary at three different orbital phases.

6 CHARATERIZATION OF THE ROSSITER–MCLAUGHLIN EFFECT OF THE G-STAR

As already mentioned in Section 4, the RV curve of the G-star shows a small RM effect (Rossiter 1924; McLaughlin 1924) at phase 0.5. This red/blueshifted distortion at the secondary eclipse is due to selective blocking of the light of the rotating star during an eclipse. When the primary star covers the blueshifted (redshifted) half of the stellar disc, the integrated light of the secondary appears redshifted (blueshifted). Because of this selective blocking of the stellar surface during the eclipse, a skewed line profile is created. This change in line profile shape results in a shift in RV, which in turn results in the redshift–blueshift distortion seen during the eclipse. The effect mainly depends on the projected rotation velocity of the star, the ratio of stellar radii, the orbital inclination and the limb darkening. To analyse this effect, we have subtracted the orbital solution (solid curve in Fig. 7) from the RV measurements of the G-star. The orbit-subtracted RV residuals are shown in Fig. 11. We used the analytical description of this effect given in Giménez (2006) to simulate the RM effect. The ratio of the stellar radii $r_{\mathrm{B}}/r_{\mathrm{G}}$, the inclination and the radius of the G-star relative to the size of the orbit r_{G} were taken from our final orbital solution. The equatorial rotational velocity of the star was set to $44 \pm 4\,\mathrm{km\,s^{-1}}$. The rotational axis of the G-star is assumed to be perpendicular to the orbital plane.

The result of our best fit is seen in Fig. 11. With our current input parameters, we cannot fully explain the RM effect. A possible

Table 8. Parameters of AU Mon together with their formal 3σ uncertainties (standard deviations) resulting from the combined PHOEBE solution for photometry and RVs.

Parameter	Value	Uncertainty
HJD_0 (245 0000.+)	4136.6734	0.0002
P_{orb} (d)	11.113 0374	0.000 0001
i (°)	78.6	0.6
q	0.17[a]	0.03
γ (km s^{-1})	17.8	0.6
A ($R_\odot$)	42	1
e	0.01	0.03
$T_{eff.B}$ (K)	14 595	900
$T_{eff.G}$ (K)	5750[a]	–
Ω_B	7.8	0.9
Ω_G	2.12	0.06
F_B	4.8	0.9
$[L_B/(L_B+L_G)]_V$	0.82	0.09
$[L_B/(L_B+L_G)]_{CoR}$	0.84	0.09
G_B	1.0[b]	–
G_G	0.9[b]	–
A_B	1.0[b]	–
A_G	0.5[b]	–
x_B (V)	0.458[b]	0.001
x_B (CoR)	0.304[b]	0.001
x_G (V)	0.465[b]	0.001
x_G (CoR)	0.542[b]	0.001
y_B (V)	0.236[b]	0.001
y_B (CoR)	0.195[b]	0.001
y_G (V)	0.243[b]	0.001
y_G (CoR)	0.243[b]	0.001
Roche radii (in units of orbital separation)		
r_B (pole)	0.12	0.02
r_B (point)	0.14	0.02
r_B (side)	0.14	0.02
r_B (back)	0.14	0.02
r_G (pole)	0.22	0.02
r_G (point)	0.31	0.02
r_G (side)	0.23	0.02
r_G (back)	0.26	0.02
Absolute dimensions		
$\log g_B$	3.78	0.09
$\log g_G$	2.50	0.03
$M_{bol,B}$ (mag)	−3.1	0.6
$M_{bol,G}$ (mag)	−0.25	0.11
M_B ($M_\odot$)	7.0	0.5
M_G ($M_\odot$)	1.2	0.3
R_B ($R_\odot$)	5.6	0.8
R_G ($R_\odot$)	10.0	0.8

[a] Adopted from spectroscopy
[b] Assumed

explanation is that we are primarily not dealing with rotational effects but with the fact that the photocentre and gravity centre of the Roche lobe filling star (G-star) are not identical and coinciding. Wilson, Pettera & van Hamme (1985) pointed out that this could also cause such distortions in the RVs during an eclipse. Another explanation comes from the fact that we have circumstellar matter together with the matter circulating from the G- to the B-component which has not been taken into account in the calculations. In order to check this, we have set the relative radius of the G-star r_G as a free parameter. The result is that we could fit the RM effect if we increase r_G to $0.44A$ (see Fig. 11).

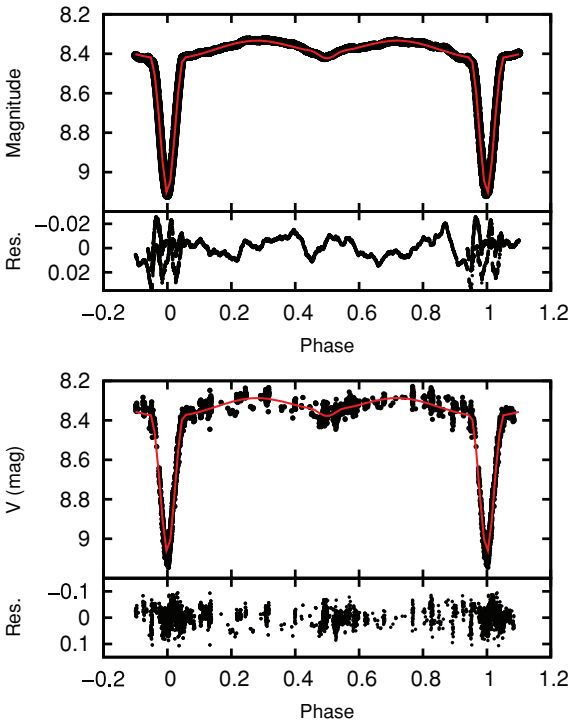

Figure 8. The final PHOEBE model plotted in red on top of one part of the CoRoT light curve (top panel) and the V-band light curve (bottom panel), after removal of the long-term period of $P_{long} = 417 \pm 8$ d, phased against the period of 11.113 0374 days. Below each light curve, the residuals of the model and observations are shown.

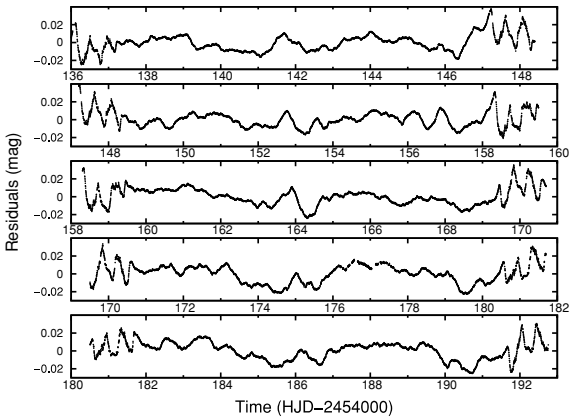

Figure 9. The O − C residuals from the final solution shown for the complete CoRoT light curve.

7 VARIATIONS ON OTHER TIME-SCALES

As Fig. 9 clearly shows a systematic pattern of rapid light changes which is most pronounced near the phases of primary eclipse was detected by CoRoT at every orbital cycle. This is also the reason why the O − C calculated from our final ephemeris for these minima are significantly larger than their accuracy (see Table 3). The fast changes near the primary eclipse are reminiscent of what Pavlovski et al. (2006) found for W Cru (most evident in the U-filter). In accordance with them, we propose that the variations are due to a non-uniform brightness distribution, probably seated in the accretion disc. We also note that the Hα profiles from very similar

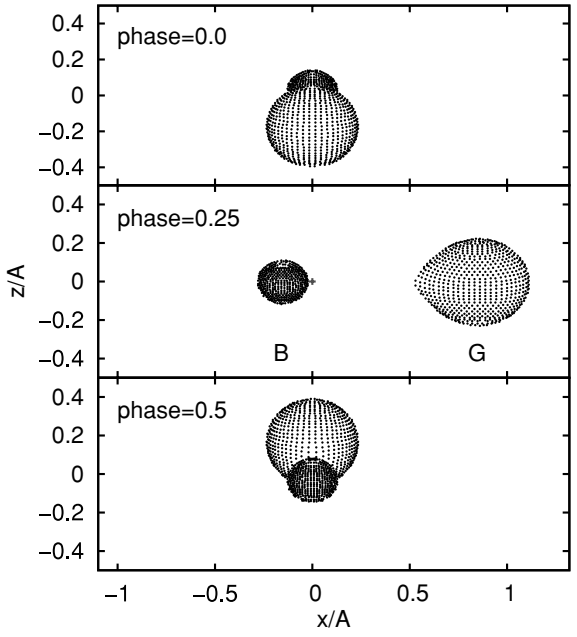

Figure 10. Representation of the B- and G-star of AU Mon pictured in three different phases. The cross in the middle panel denotes the centre of mass. The system does not show a total eclipse.

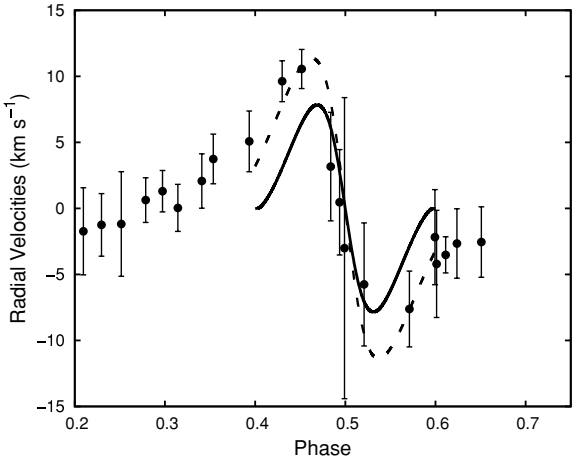

Figure 11. The orbit subtracted RV residuals (dots) showing the RM effect at phase 0.5. The solid line is the simulation of the RM effect with the parameters given in the text, the dashed line shows the RM effect after an increase of the radius of the G-star.

orbital phases but from two different orbital cycles differ from each other (see Fig. 12). For instance, the additional redshifted absorption feature is more pronounced in the first cycle than in the last one.

As already mentioned in Section 2.2, Peters (1994a,b) suggested that the cyclic variations in the mass transfer rate could be due to pulsations of the mass-losing secondary. In order to investigate this we performed a frequency analysis on the residuals of the light curve after subtracting our final PHOEBE model shown in Fig. 8.

The periodogram of the residual data set is completely contaminated by the binary orbital frequency and its harmonics. As can be seen in Figs 8 and 9, the residuals of the CoRoT data near the phase of primary minimum show much larger variations than the residuals outside eclipse. This periodicity is due to the fact that the primary

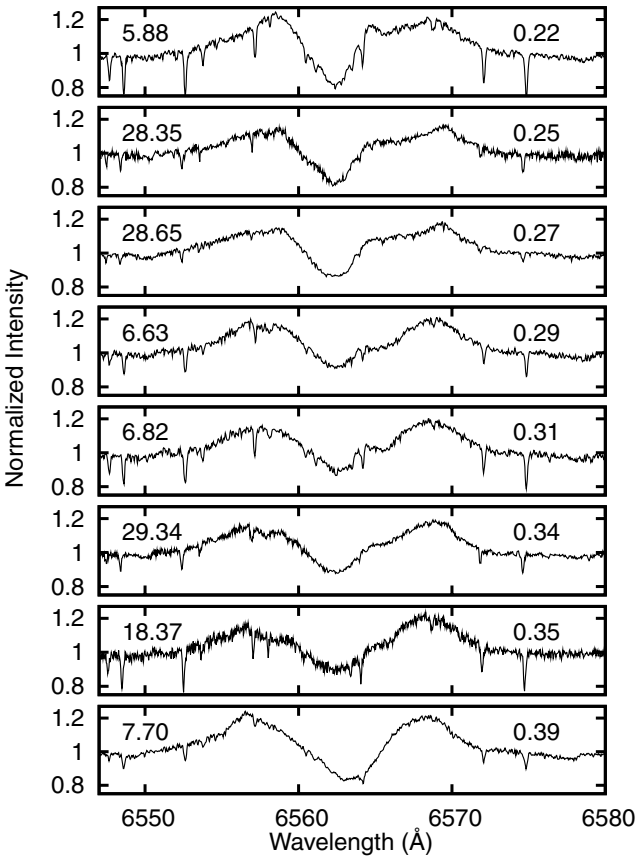

Figure 12. A sequence of the Hα line profiles showing a complicated velocity field and cycle-to-cycle variations. Data from three consecutive orbital cycles can be seen. In the left corner of each plot, we list the time of measurement (HJD 2454 100) and in the right corner we give the orbital phase calculated from ephemeris (2).

minima are not completely well fitted, thus introducing a strong signal with the orbital frequency of 11.113 03 days. In order to avoid this, we did not consider the residuals during the phase of primary eclipse and recomputed the FT. The result is shown in Fig. 13. The orbital frequency and its harmonics are still present (from 0 to 3 d^{-1}) in the top periodogram. The frequency peaks in the range of 12–17 d^{-1} are due to the CoRoT satellite orbital frequency ($f_{\rm orb,CoR} = 13.97\,{\rm d}^{-1}$) and are thus instrumental. We searched for frequencies using the PDM method (Stellingwerf 1978) and pre-whitened the data for the orbital frequency and eight other low-frequency signals ($<0.2\,{\rm d}^{-1}$) using a spline fit to the bin means (see e.g. Waelkens & Rufener 1983). This resulted in a residual light curve without the binary and satellite signature.

The residuals from the PDM pre-whitening procedure were analysed using the short-time Fourier transform (STFT) with a Hamming window (Harris 1978). The result can be seen in Fig. 14. The STFT was calculated using a window width of 10 days, and evaluated in 100 equidistant time points. The peaks at 10.4 (f_1) and 8.3 d^{-1} (f_2) are clearly visible as nearly continuous frequency bands. A short drop in amplitude is notable in the 8.3 d^{-1} frequency band around day $\tau = 38$ d. The power excess at lower frequency cannot be attributed to one or several stable frequencies. Instead, the time-dependent behaviour of low frequencies with short-living amplitudes are visible, resulting in a smeared out region of power excess in a full Scargle periodogram (see the middle panel of Fig. 13). It is difficult to draw firm conclusions about the origin of these

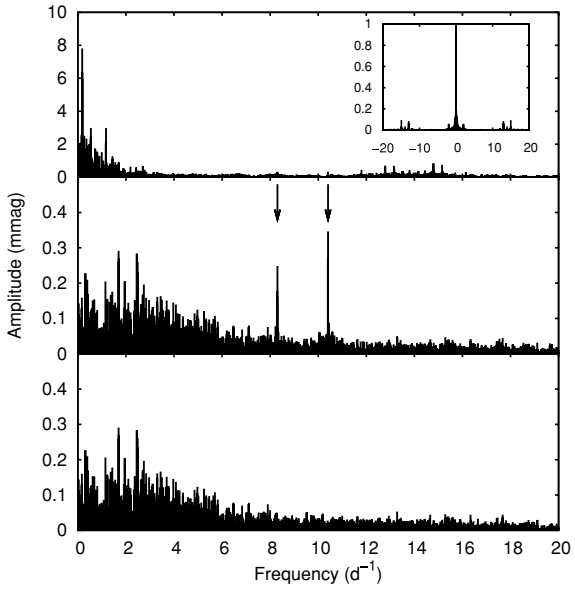

Figure 13. The periodogram of the residuals out of primary eclipse together with the spectral window (top panel + inset). The middle panel shows the periodogram after pre-whitening for nine low-frequency signals. The bottom panel shows the final residual periodogram after pre-whitening all significant frequency peaks.

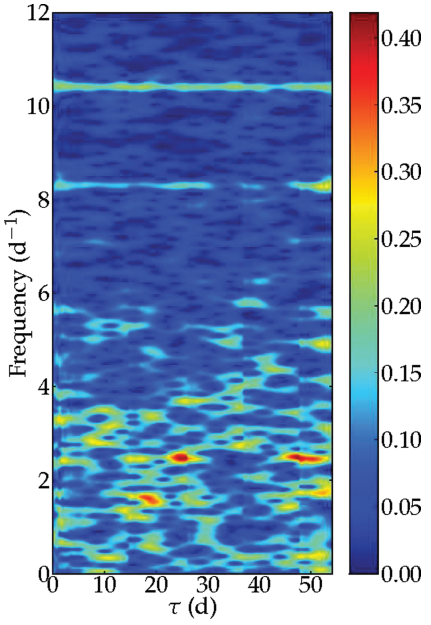

Figure 14. The STFT of the residuals of the CoRoT light curve after pre-whitening for the orbital frequency. The units of the colour scale are in mmag. See the text for details.

features, due to the added uncertainties from the PDM pre-whitening method in this frequency band. However, the two frequencies in Table 9 are unaffected by our PDM pre-whitening method, and are definitely present in the Scargle periodogram. Their characteristics are listed in Table 9. Since these frequencies are not detectable in the spectra, we cannot directly assign a physical origin to them. The frequencies f_1 and f_2 are likely to originate from the B-star because it produces ∼82 per cent of the light and concerns isolated frequency peaks. Although, theory does not predict such pulsations for B-stars (see e.g. Miglio, Montalbán & Dupret 2007), such frequencies have

Table 9. Frequencies found in the residuals together with their S/N ratio (we refer to the text for explanation).

ID	Frequency		Amplitude	S/N
	(d^{-1})	(μHz)	(mmag)	
f_1	10.4081	120.46	0.34	14.8
f_2	8.3033	96.10	0.25	9.2

Note. The error estimate (Montgomery & O'Donoghue 1999) for the frequencies is $\pm$ 0.0002 d^{-1}. The error on the amplitude is 0.01 mmag.

also been detected in CoRoT data of the Be star HD 49330 (Huat et al. 2009). This result puts AU Mon in the neighbourhood of the sample of semidetached Algol-type eclipsing binaries with an oscillating mass accreting component (oEA stars, with RZ Cas as the best-studied object; Mkrtichian et al. 2007). AU Mon cannot be fully classified as an oEA star, because oEA stars are at the end of the mass transfer regime which is still not the case for AU Mon.

On the other hand, theory predicts that the G-star should produce solar-like oscillations (see e.g. Houdek & Gough 2002; Samadi et al. 2007). Since we know the mass, radius and $T_{\rm eff}$ of the star, we predict $\nu_{\rm max} = M_{\rm G}/R_{\rm G}^2 \times (T_{{\rm eff},G}/5777)^{-0.5} \times 3050 \approx 34$ μHz (=2.94 d^{-1}) to be the frequency at which to expect such oscillations (Kjeldsen & Bedding 1995). This value is in agreement with the location of the power excess in the Scargle periodogram of AU Mon (middle panel of Fig. 13). The amplitude of the power excess is not in disagreement with the amplitudes of the discovered solar-like oscillations in the CoRoT data of red giants (De Ridder et al. 2009) taking into account the flux contribution of the G-star. Due to a lack of mode identification and uncertainty on the origin of the oscillations, we are unable to exploit the detected frequencies seismically without additional spectroscopic information about them.

8 UNDERSTANDING THE LONG-TERM LIGHT VARIATIONS

Other cases than AU Mon exist in which the discovery of long-term periodic or at least cyclic brightness variations (reminiscent of AU Mon) have been claimed, namely those cases where systematic photometry in a calibrated photometric system has been carried out or where interacting binaries with Balmer emission lines and hot mass-gaining components are discussed. Probably, the first reports of such a behaviour are RX Cas (Kalv 1979), TV Cas = HD 1486 (Walter 1979) and V505 Sgr = BD−14° 5578 (Walter 1981). However, the latter two systems exhibit only very faint single-peaked Hα emission and their long-term variations are probably related to the presence of distant third components in these systems (Richards & Albright 1999; Vesper, Honeycutt & Hunt 2001).

In Table 10, we provide basic information on Galactic emission-line systems with cyclic long-term variability known to us. During the past 5 years, similar systems were also discovered and studied rather intensively in the Magellanic Clouds (Mennickent et al. 2003, 2005a,b; Mennickent, Assmann & Sabogal 2006; Mennickent et al. 2008). In spite of all effort, the true cause of the long-term cyclic changes remains unexplained, although several different interpretations were put forward: Kalv (1979) interpreted the 516-day periodicity of RX Cas as pulsation of the Roche lobe filling star. Harmanec et al. (1996) considered the possibility that the 282-day cycle of β Lyr is a beat period between the orbital period and rapid changes with a cycle of $4\overset{\rm d}{.}7$ which they detected in spectroscopy. They also pointed out some similarity with the 164-day cycle of V1343 Aql = SS 433, a massive $13\overset{\rm d}{.}08$ X-ray binary with

Table 10. Galactic hot emission-line binaries with cyclic long-term brightness changes. The tabulated mass ratio is always the ratio of the mass of the lighter (usually Roche lobe filling) component to that of the B-star.

Name	BD	$P_{\rm orb.}$	$P_{\rm long}$	Mass ratio	References
RX Cas	$+67^\circ$ 244	$32\overset{\rm d}{.}312$	$516\overset{\rm d}{.}06$	0.30 ± 0.05	1, 2, 3, 4
AU Mon	-01° 1449	$11\overset{\rm d}{.}113$	$417\overset{\rm d}{.}0$	0.17 ± 0.03	5
CX Dra	$+52^\circ$ 2280	$6\overset{\rm d}{.}696$	$130^{\rm d}$–$180^{\rm d}$	0.23	6, 7, 8
β Lyr	$+33^\circ$ 3223	$12\overset{\rm d}{.}94$	$282\overset{\rm d}{.}37$	0.225	8, 9, 10
V360 Lac	$+41^\circ$ 4623	$10\overset{\rm d}{.}085$	$322\overset{\rm d}{.}24$	0.163	11, 12

References to original studies identified by the running numbers in column 'References':
1 – Kalv (1979); 2 – Křiž et al. (1980); 3 – Andersen et al. (1989); 4 – Pustylnik, Kalv & Harvig (2007); 5 – this study; 6 – Koubský et al. (1980); 7 – Horn et al. (1992); 8 – Richards et al. (2000); 9 – Harmanec et al. (1996); 10 – Harmanec (2002) 11 – Hill et al. (1997); 12 – Linnell et al. (2006).

bipolar jets. Wilson & van Hamme (1999) also studied β Lyr. They concluded that neither apsidal advance nor precession can account for the 282-day light variation. They were unable to exclude pulsations of the disc as the cause. As already mentioned, Peters (1991) concluded that the optical brightness variations of AU Mon are due to a 1200 K variation in the photospheric effective temperature of the B primary.

Mennickent et al. (2003) reported the discovery of eclipsing binaries with long-term periodic brightness changes from Optical Gravitational Lensing Experiment (OGLE) photometry of the Magellanic Clouds. Mennickent et al. (2003) pointed out that the light maxima of the long cycles are always accompanied by a mild reddening of the objects in question. Mennickent et al. (2005b) concluded that the long brightness changes are often cyclic rather than strictly periodic ones. Subsequently, Mennickent et al. (2008) concluded that the long-term variations must be due to variations in *circumbinary* matter as we found for AU Mon. They suggested that the system experiences supercycles of mass outflow which lead to replenishment of the circumbinary envelope.

AU Mon may become a key object to study the true nature of the long-term brightness changes since it is bright and the amplitude of the 417-day period is large. In spite of our effort to collect and homogenize existing photometry, available material on colour variations is, unfortunately, very scarce. In Fig. 3, we compare the V magnitude and $B - V$ and $U - B$ colour changes along the 417-day cycle for all observations we were able to transform into comparable *UBV* magnitudes. Unfortunately, there is no colour information near phases of the brightness maximum. A plot of both colour indices versus time shows that there could also be colour variations on longer time-scales than those related to the 417-day cycle. If this is a more general pattern, this could perhaps also explain somewhat contradictory reports on the colour behaviour of various objects studied by Mennickent and his collaborators. Clearly, future systematic calibrated multicolour photometry of AU Mon over the whole 417-day cycle is very desirable.

We tentatively suggest that the long-term brightness changes of AU Mon must be associated with some circumbinary matter and it is plausible to assume that the bulk of such material is associated with putative bipolar jets for which we find indirect support from the shift of the RV curves of some spectral lines associated with the B-star. Bisikalo et al. (2000) showed via hydro calculations for β Lyr that when the encircling stream hits the denser primary stream from the mass-losing star, it gets bended and goes out of the orbital plane resulting in jet-like structures. Peters (2007) reported probable detections of bipolar jets of very hot plasma, perpendicular to the orbital plane, for three other hot interacting binaries: TT Hya; V356 Sgr and RY Per. However, Miller et al. (2007) studied circumstellar matter of TT Hya and argued against jets. The variations themselves could have two possible causes: either cyclic changes in the mass outflow from the binary as suggested by Mennickent et al. (2008) or precession of the binary orbit which would change the attenuation of the binary due to changing projection effects of jets. This latter idea seems improbable, however, in the light of our finding that the light curve from the maxima and minima of the 417-day period lead to the same binary elements including the orbital inclination. It is clear that continuing systematic observations of AU Mon, including spectrointerferometry and polarimetry, could help to understand the nature of the remarkable changes of these interesting objects.

9 SUMMARY

Our analyses of very accurate CoRoT space photometry, past Johnson V photoelectric photometry and high-resolution echelle spectra led to the determination of improved fundamental stellar properties of both components of the massive and interacting system AU Mon. We derived new and accurate ephemerides for both the orbital motion (with a period of $11\overset{\rm d}{.}113\,0374$) and the long-term, overall brightness variation (with a period of $416\overset{\rm d}{.}9$). It is shown that this long-term variation must be due to attenuation of the total light by some variable circumbinary material. We derived the binary mass ratio $M_{\rm G}/M_{\rm B} = 0.17 \pm 0.03$. Using this value of the mass ratio as well as the RVs of the G-star, we obtained a consistent and coherent light curve solution and a new estimate of the stellar masses, radii, luminosities and the effective temperatures.

We must point out that our final model does not include the gas stream and accreting matter on the B-star. It would be interesting to consider such complications in any future modelling of the binary. We also report the discovery of rapid and periodic light changes visible in the high-quality residual CoRoT light curves. The rapid light changes visible in the residuals near primary minima repeat at every orbital period. They are probably due to a non-uniform brightness distribution, seated in the accretion disc. Outside the primary minima of the CoRoT light curve, we detect two frequencies, they are in the expected frequency domain of B-stars. Complementary interferometric and polarimetric observations will be needed to even better understand the geometry and the nature of the circumbinary matter in AU Mon.

ACKNOWLEDGMENTS

The authors acknowledge critical remarks and useful suggestions by Dr. Johannes Andersen on an earlier version of the paper. YF thanks P. Hadrava for making his KOREL computer code (Release 2.12.04) available to him. We also thank P. Hadrava for the use of his FOTEL computer code. This research has received funding from the European Research Council under the European Community's Seventh Framework Programme (FP7/2007–2013)/ERC grant agreement n°227224 (PROSPERITY), as well as from the Research Council of K.U. Leuven grant agreement GOA/2008/04. MB is Postdoctoral fellow of the Fund for Scientific Research, Flanders. The research of PH was supported by the grants 205/06/0304 and 205/08/H005 of the Czech Science Foundation and also from the Research Programme MSM0021620860 *Physical study of objects and processes in the solar system and in astrophysics* of the Ministry of Education of the Czech Republic. The FEROS data are being obtained as part of the ESO Large Programme: LP178.D-0361 (PI: Poretti). This work was supported by the Italian ESS project, contract ASI/INAF I/015/07/0, WP 03170. KU acknowledges financial support from

a *European Community Marie Curie Intra-European Fellowship*, contract number MEIF-CT-2006-024476. PJA acknowledges financial support from a 'Ramón y Cajal' contract of the Spanish Ministry of Education and Science. We acknowledge the use of the electronic data base SIMBAD operated by the CDS, Strasbourg, France and the electronic bibliography maintained by the NASA/ADS system. Finally, we thank Andrea Miglio for valuable discussions on stellar oscillations.

REFERENCES

Andersen J., Pavlovski K., Piirola V., 1989, A&A, 215, 272
Bisikalo D., Matsuda T., 2007, in Hartkopf W. I., Guinan E. F., Harmanec P., eds, Proc. IAU Symp. 240, Testing and Improving the Dynamical Theory of Mass Exchange. Cambridge Univ. Press, Cambridge, p. 356
Bisikalo V. V., Boyarchuk A. A., Harmanec P., Hadrava P., Kuznetsov O. A., 2000, in Smith M. A., Henrichs H. F., Fabregat J., eds, ASP Conf. Ser. Vol. 214, The Be Phenomenon in Early-Type Stars. Astron. Soc. Pac., San Francisco, p. 697
Castelli F., Gratton R. G., Kurucz R. L., 1997, A&A, 318, 841
Castelli F., Kurucz R. L., 2003, in Piskunov N., Weiss W. W., Gray D. F., eds, Proc. IAU Symp. 210 Modelling of Stellar Atmospheres. Cambridge Univ. Press, Cambridge, p. 20
Castelli F., Kurucz R. L., 2004, preprint (astro-ph/0405087)
Cerruti-Sola M., Lorenzi L., 1977, Inf. Bull. Var. Stars, 1348, 1
David M., Verschueren W., 1995, A&AS, 111, 183
De Ridder J. et al., 2009, Nat, 459, 398
Egikyan A. G., 1989, Astrophy., 30, 407
Elias N. M. II, 1990, ApJ, 352, 300
Florja N. T., 1937, Trudy Gosud. Astron. Inst. P.K. Sternberga, 8, 2
Fridlund M., Baglin A., Lochard J., Conroy L., 2006, ESA Special Publication, 1306, 1
Giménez A., 2006, ApJ, 650, 408
Giuricin G., Mardirossian F., Mezzetti M., 1982, MNRAS, 199, 131
Glazunova L. V., Yushchenko A. V., Tsymbal V. V., Mkrtichian D. E., Lee J. J., Kang Y. W., Valyavin G. G., Lee B.-C., 2008, AJ, 136, 1736
Hadrava P., 1990, Contr. Astron. Obser. Skalnaté Pleso, 20, 23
Hadrava P., 1995, A&AS, 114, 393
Hadrava P., 1997, A&AS, 122, 581
Hadrava P., 2004a, Publ. Astron. Inst. Acad. Sci. Czech Rep., 92, 1
Hadrava P., 2004b, Publ. Astron. Inst. Acad. Sci. Czech Rep., 92, 15
Harmanec P., 1988, Bull. Astron. Instit. Czechoslovakia, 39, 329
Harmanec P., 1990, A&A, 237, 91
Harmanec P., 1998, A&A, 335, 173
Harmanec P., 2001, Publ. Astron. Inst. Czechoslovak Acad. Sci., 89, 9
Harmanec P., 2002, Astron. Nachrichten, 323, 87
Harmanec P., 2003, Publ. Canakkale Onsekiz Mart Univ., 3, 221
Harmanec P., Božić H., 2001, A&A, 369, 1140
Harmanec P. et al., 1996, A&A, 312, 879
Harris F. J., 1978, Proc. IEEE, 66, 51
Hill G., Harmanec P., Pavlovski K., Božic H., Hadrava P., Koubský P., Žižňovský J., 1997, A&A, 324, 965
Hoffmeister C., 1931, Astron. Nachrichten, 242, 129
Horn J., Hubert A. M., Hubert H., Koubský P., Bailloux N., 1992, A&A, 259, L5
Horn J., Kubát J., Harmanec P., Koubský P., Hadrava P., Šimon V., Štefl S., Škoda P., 1996, A&A, 309, 521
Houdek G., Gough D. O., 2002, MNRAS, 336, L65
Huat L. et al., 2009, A&A, in press
Hubeny I., Lanz T., 1995, ApJ, 439, 875
Kalv P., 1979, Tartu Astrofuusika Obser. Teated, 58, 3
Kaufer A., Stahl O., Tubbesing S., Nørregaard P., Avila G., Francois P., Pasquini L., Pizzella A., 1999, The Messenger, 95, 8
Kaufer A., Wolf B., Andersen J., Pasquini L., 1997, The Messenger, 89, 1
Kilkenny D., Whittet D. C. B., Davies J. K., Evans A., Bode M. F., Robson E. I., Banfield R. M., 1985, South African Astron. Obser. Circular, 9, 55
Kjeldsen H., Bedding T. R., 1995, A&A, 293, 87
Koubský P., Harmanec P., Horn J., Žďárský F., Jerzykiewicz M., Kříž S., Papousek J., Pavlovski K., 1980, Bull. Astron. Inst. Czechoslovakia, 31, 75
Kreiner J. M., 2004, Acta Astron., 54, 207
Kříž S. et al., 1980, Bull. Astron. Inst. Czechoslovakia, 31, 284
Lause F., 1938, Krakow Obs. Int. Suppl., 16, 59
Linnell A. P. et al., 2006, A&A, 455, 1037
Lorenzi L., 1977, A&A, 55, 295
Lorenzi L., 1980a, A&A, 85, 342
Lorenzi L., 1980b, A&AS, 40, 271
Lorenzi L., 1982, Acta Astron., 32, 431
Lorenzi L., 1985, Inf. Bull. Var. Stars, 2704, 1
Lucy L. B., Sweeney M. A., 1971, AJ, 76, 544
McLaughlin D. B., 1924, ApJ, 60, 22
Manfroid J. et al., 1991, A&AS, 87, 481
Mennickent R. E., Pietrzyński G., Diaz M., Gieren W., 2003, A&A, 399, L47
Mennickent R. E., Assmann P., Pietrzyński G., Gieren W., 2005a, in Sterken C., ed., ASP Conf. Ser. Vol. 335, The Light-Time Effect in Astrophysics. Astron. Soc. Pac., San Francisco, p. 129
Mennickent R. E., Cidale L., Díaz M., Pietrzyński G., Gieren W., Sabogal B., 2005b, MNRAS, 357, 1219
Mennickent R. E., Assmann P., Sabogal B., 2006, Rev. Mexicana Astron. Astrofisica, 26, 173
Mennickent R. E., Kołaczkowski Z., Michalska G., Pietrzyński G., Gallardo R., Cidale L., Granada A., Gieren W., 2008, MNRAS, 389, 1605
Miglio A., Montalbán J., Dupret M.-A., 2007, MNRAS, 375, L21
Miller B. P., Budaj J., Richards M. T., 2005, AAS, 37, 486
Miller B. P., Budaj J., Richards M. T., Koubský P., Peters G. J., 2007, ApJ, 656, 1075
Mkrtichian D. E. et al., 2007, 370, 194
Montgomery M. H., O'Donoghue D., 1999, Delta Scuti Star Newsletter, 13, 28
Pavlovski K., Burki G., Mimica P., 2006, A&A, 454, 855
Perruchot S. et al., 2008, SPIE Conf. Ser., 7014, 1
Perryman M. A. C., ESA, 1997, The HIPPARCOS and TYCHO catalogues. ESA, Noordwijk
Peters G., 2007, in Hartkopf W. I., Guinan E. F., Harmanec P., eds, Proc. IAU Symp. 240, Testing and Improving the Dynamical Theory of Mass Exchange. Cambridge Univ. Press, Cambridge, p. 148
Peters G. J., 1988, IUE Proposal, 3160
Peters G. J., 1991, BAAS, 23, 902
Peters G. J., 1994a, IUE Proposal, 4820
Peters G. J., 1994b, in Peters G. J., ed., ASP Conf. Ser. Vol. 56, Interacting Binary Stars. Astron. Soc. Pac., San Francisco, p. 384
Peters G. J., 1996, BAAS, 28, 757
Peters G. J., Polidan R. S., 1982, in Jaschek M., Groth H.-G., eds, Proc. IAU Symp. 98, Be Stars. Cambridge Univ. Press, Cambridge, p. 405
Peters G. J., Polidan R. S., 1998, ApJ, 500, L17
Pfeiffer M. J., Frank C., Baumueller D., Fuhrmann K., Gehren T., 1998, A&AS, 130, 381
Plavec M., Koch R. H., 1978, Inf. Bull. Var. Stars, 1482, 1
Plavec M. J., Popper D. M., Ulrich R. K., 1980, in Plavec M. J., Popper D. M., Ulrich R. K., eds, Proc. IAU Symp. 88, Close Binary Stars: Observations and Interpretation. Cambridge Univ. Press, Cambridge, p. 251
Polidan R. S., Peters G. J., 1982, Advances Ultraviolet Astron., 534
Popper D. M., 1962, PASP, 74, 129
Popper D. M., 1989, ApJS, 71, 595
Prša A., Zwitter T., 2005, ApJ, 628, 426
Pustylnik I., Kalv P., Harvig V., 2007, Astron. Astrophys. Trans., 26, 31
Richards M. T., Albright G. E., 1999, ApJS, 123, 537
Richards M. T., Koubský P., Šimon V., Peters G. J., Hirata R., Škoda P., Masuda S., 2000, ApJ, 531, 1003
Roberts D. H., Lehar J., Dreher J. W., 1987, AJ, 93, 968
Rossiter R. A., 1924, ApJ, 60, 15
Royer F., Grenier S., Baylac M.-O., Gómez A. E., Zorec J., 2002, A&A, 393, 897

Sahade J., Cesco C. U., 1945, ApJ, 101, 235
Sahade J., Ferrer O. E., 1982, PASP, 94, 872
Sahade J., Ferrer O., Garcia L. G., Brandi E., Barba R., 1997, PASP, 109, 1237
Samadi R., Georgobiani D., Trampedach R., Goupil M. J., Stein R. F., Nordlund Å., 2007, A&A, 463, 297
Schaller G., Schaerer D., Meynet G., Maeder A., 1992, A&AS, 96, 269
Škoda P., 1996, in Jacoby G. H., Barnes J., eds, ASP Conf. Ser. Vol. 101, Astronomical Data Analysis Software and Systems V. Astron. Soc. Pac., San Francisco, p. 187
Stellingwerf R. F., 1978, ApJ, 224, 953
Uytterhoeven K. et al., 2008, J. Phys. Conf. Ser., 118, 012077
van Hamme W., 1993, AJ, 106, 2096
Vesper D., Honeycutt K., Hunt T., 2001, AJ, 121, 2723
Vivekananda Rao P., Sarma M. B. K., 1998, A&AS, 128, 441
Vučković M., Aerts C., Østensen R., Nelemans G., Hu H., Jeffery C. S., Dhillon V. S., Marsh T. R., 2007, A&A, 471, 605
Waelkens C., Rufener F., 1983, A&A, 119, 279
Walter K., 1979, A&AS, 37, 493
Walter K., 1981, A&A, 101, 369
Wilson R. E., 1990, ApJ, 356, 613
Wilson R. E., 1994, PASP, 106, 921
Wilson R. E., Devinney E. J., 1971, ApJ, 166, 605
Wilson R. E., van Hamme W., 1999, MNRAS, 303, 736
Wilson R. E., Pettera L. E., van Hamme W., 1985, ApJ, 289, 748
Zucker S., Mazeh T., 1994, ApJ, 420, 806

APPENDIX A: TIMES OF MINIMA

Table A1. Visual, photographic, photoelectric and CCD times of minima.

Time (HJD 240 0000)	O − C	Type	Time (HJD 240 0000)	O − C	Type
26743.160	0.124	vis	37378.364	0.151	pg
26743.390	0.354	pg	37400.351	−0.088	pg
26765.320	0.058	pg	37578.633	0.385	pg
26976.400	−0.010	vis	37667.505	0.353	pg
26987.530	0.007	vis	38322.601	−0.220	pg
27076.430	0.003	vis	38378.568	0.182	pg
27120.890	0.011	vis	38411.508	−0.217	pg
27487.583	−0.027	vis	38467.353	0.062	pg
27843.110	−0.117	vis	38856.363	0.116	pg
27887.631	−0.048	vis	39200.388	−0.363	pg
27932.230	0.099	pg	39945.411	0.086	pg
28209.912	−0.045	vis	40478.609	−0.141	pg
28498.919	0.023	vis	40656.362	−0.197	pg
28543.377	0.029	vis	41056.332	−0.296	pg
28921.155	−0.037	vis	41334.391	−0.063	pg
28954.480	−0.051	vis	41356.438	−0.242	pg
28965.656	0.012	vis	41367.466	−0.327	pg
30021.380	−0.002	pg	41390.355	0.335	pg
30810.400	−0.008	pg	42090.373	0.232	pg
31910.610	0.011	pg	42790.2350	−0.027	pe
32888.560	0.014	pg	42801.3602	−0.015	pe
33266.400	0.011	pg	42868.1210	0.068	pe
33533.160	0.058	pg	42879.2360	0.069	pe
34444.380	0.009	pg	43123.653	−0.000	UBV
34811.100	−0.001	pg	43190.332	0.001	UBV
35044.500	0.025	pg	43201.449	0.005	UBV
35900.386	0.207	pg	48502.220	−0.143	V
37367.333	0.233	pg	51513.5290	−0.468	ccd

Note. The times were adopted form the General Search Gateway of the Variable-Star Section of the Czech Astronomical Society (http://var.astro.cz/gsg). The O − C values were calculated with our new ephemeris (2) for AU Mon. The third column lists the type of observation. vis: visual; pg: photographic; pe: photoelectric.

APPENDIX B: AVAILABLE PHOTOELECTRIC DATA

Table B1. Excerpt of the available photoelectric observations of AU Mon. The full table is available as Supporting Information.

Data from Lorenzi (1985)	
Time (HJD 240 0000)	*V* (mag)
45 343.4114	8.380
45 346.3339	9.137
45 346.4262	9.048
45 351.4059	8.415
45 351.4202	8.418
45 353.3960	8.391
45 354.4253	8.387
45 355.3607	8.385
45 356.3518	8.448
45 357.2635	9.118
45 357.2823	9.151
45 357.3028	9.165
45 357.3205	9.181
45 357.3349	9.180
45 357.3471	9.187
45 357.3600	9.188
45 357.3739	9.185
45 357.3927	9.192
45 357.4045	9.180
45 357.4161	9.169
45 357.4287	9.165
45 357.4403	9.155
45 357.4565	9.147

SUPPORTING INFORMATION

Additional Supporting Information may be found in the online version of this article:

Table B1. Available photoelectric observations of AU Mon.

Please note: Wiley-Blackwell are not responsible for the content or functionality of any supporting materials supplied by the authors. Any queries (other than missing material) should be directed to the corresponding author for the article.

This paper has been typeset from a TEX/LATEX file prepared by the author.